Reprinted from The Journal of Physical Chemistry, 1995, 99.

Transient Grating Optical Heterodyne Detected Impulsive Stimulated Raman Scattering in Simple Liquids

Peter Vöhringer[†] and Norbert F. Scherer*[,‡]

Department of Chemistry, University of Pennsylvania, Philadelphia, Pennsylvania 19104-6323

Received: July 25, 1994; In Final Form: September 27, 1994[⊗]

The real and imaginary parts of individual tensor elements of the nonresonant third-order nonlinear optical susceptibility of simple liquids, carbon tetrachloride and benzene, have been characterized for the first time by transient grating optical heterodyne detected impulsive stimulated Raman scattering (TG-OHD-ISRS). Optical heterodyning is achieved through additional scattering induced by a thermal grating. Vibrational modes to 1000 cm^{-1} are impulsively prepared and probed using 15 fs laser pulses. This technique allows for a precise determination of frequencies and dephasing times of intramolecular Raman-active vibrations. It is shown that the symmetry of these modes defines the measured phase of the oscillatory modulations of the various linearly detected tensor components of $\chi^{(3)}(t)$. Advantages to conventional techniques, such as optical heterodyne detected Raman induced Kerr effect spectroscopy or homodyne detected impulsive stimulated Raman scattering, are demonstrated. Further detection of the real or imaginary part of the susceptibilities using phase locked femtosecond optical pulses is discussed.

I. Introduction

The energetics and dynamics of chemical reactions occurring in condensed media are affected by various solvent (or host) properties. Barrier heights along the reaction coordinate may be altered by the solvent dielectric constant or polarizability[1] whereas the dynamics can be altered by the frequency-dependent response of the medium.[2] The spectrum of solvent fluctuations coupled to the reaction coordinate can be related to the force autocorrelation function of the projection of the solvent dynamics on the coordinate of interest.[3] An experimental objective[4,5] is, then, the determination of the spectrum of solvent equilibrium fluctuations and their frequency- or mode-dependent couplings, for comparison with independent measures of the reaction dynamics.

Measurement and interpretation of the intra- and intermolecular (vibrational) dynamics of neat liquids would be enhanced if the experimental method would embody several characteristics. First, the measured signal should be sensitive to the dynamical fluctuations of the medium. Second, this signal should be linearized for detection of the nonlinear optical response, and not the modulus square, thereby avoiding the detection of cross-terms between different types of motion. Third, the technique should be specific to a single tensor element of the nonlinear optical response of the medium.

Femtosecond off-resonant nonlinear spectroscopies, such as impulsive stimulated Raman scattering (ISRS) in transient grating geometries[5-8] and optical heterodyne- detected transient birefringence (i.e., Raman induced Kerr effect spectroscopy, OHD- RIKES or OHD-OKE),[9-15] can be regarded as time domain analogs of dynamic light scattering techniques (DLS).[16] Vibrational frequencies and time scales of vibrational dephasing can be inferred from spontaneous Raman spectra by analyzing peak positions and band shapes. ISRS in transient grating geometries and OHD-OKE are characterized by an "impulsive" broad-band excitation which allows for the preparation of vibrational superposition states in the electronic ground state. Consequently, the detected time-dependent third-order polarization, $P^{(3)}(t)$, exhibits underdamped sinusoidal modulations with frequencies corresponding to all Raman-active modes that are accessible within the bandwidth of the optical excitation pulse. The dephasing dynamics associated with the time evolution of the vibrational coherence state (i.e., wave packet) can be directly identified with the measured damping of the quantum beat in the femtosecond transient. It is worth pointing out that impulsive stimulated Raman scattering (ISRS) is actually the mechanism which induces coherent vibrational motion observed in either the grating geometry (TG-ISRS) or geometries employing only a single excitation beam such as OHD-OKE.

It has been shown that TG-ISRS and OHD-OKE provide valuable information about the nature of molecular dynamics in neat liquids.[8,10,17,18] In particular, detailed knowledge of very low-frequency (collective) intermolecular degrees of freedoms of the liquid as well as single-particle (diffusive) orientational motions has become accessible. Such structural changes occur on time scales ranging from subhundred femtoseconds to several picoseconds. In Rayleigh-wing spectra these dynamics give rise to a very low-intensity pedestal resulting from collision- and interaction-induced local motions with a superimposed sharp Lorentzian peak of high intensity.[19] These spectral features are often extremely difficult to analyze. By contrast, time domain measurements with sufficient time resolution clearly resolve these motions as strongly overdamped oscillations and overall exponential decays. Simple Fourier transformation of the detected OHD-OKE response allows for a precise description of the spectral density[3] of the liquid from zero to several hundered wavenumbers without the background intrinsic to frequency domain light scattering measurements.[16]

The present paper presents transient grating optical heterodyne detected impulsive stimulated Raman scattering (TG-OHD-ISRS) measurements of individual tensor elements of the nonresonant response function of a pure liquid. The technique combines the advantages of both conventional ISRS carried out in grating geometries and OHD-OKE, i.e., selectivity to individual tensor elements and linearized detection of the real part of the third-order susceptibility (polarization), respectively, thereby allowing for an independent determination of the

* To whom correspondence should be addressed.
[†] Deutsche Forschungsgemeinschaft Postdoctoral Fellow.
[‡] National Science Foundation–National Young Investigator.
[⊗] Abstract published in *Advance ACS Abstracts*, February 1, 1995.

0022-3654/95/2099-2684$09.00/0

isotropic and anisotropic parts of the nonlinear optical response. The mechanism that gives rise to optical heterodyning is shown to arise from additional diffraction that is induced by a stationary (i.e., time independent on the femto- to picosecond time scale) thermal grating. In section II of this paper we briefly describe experimental details of our laser system and optical arrangements that were used in the studies reported here. Section III presents the time resolved femtosecond OHD-OKE transient response of pure carbon tetrachloride together with TG-OHD-ISRS data for the same liquid. Analogous results are presented for liquid benzene. The results of our TG-OHD-ISRS experiments are discussed in section IV. Optical heterodyning is discussed in more detail in terms of a local oscillator originating from diffraction off the additional thermal grating. Implications to phase locked femtosecond pulse interferometry[20] are outlined.

A. Background. Impulsive stimulated scattering was first demonstrated about 10 years ago by Nelson et al. with coherent excitation of acoustic and optic phonons in liquids[21] and solids.[22] The observation of intramolecular coherences became possible with the improvement of time resolution into the sub-100 fs regime.[6] TG-ISRS is usually carried out in a three-pulse pump–probe geometry in which two pump pulses interfere in the sample to create a time dependent holographic grating that acts to diffract a variably delayed probe pulse under well-defined phase matching conditions.[5,7] Thus, the TG-ISRS transient is proportional to the modulus square of the induced third order polarization.[7] $P^{(3)}$ can be expressed in terms of the Fourier transform of the third-order nonlinear optical response $\chi^{(3)}(t)$ to represent the TG-ISRS signal as a proper convolution with the incident radiation fields E_i[23],

$$S_{\mathrm{ISRS}}(t_d) \propto \int_{-\infty}^{\infty} |E_3(t-t_d)|^2 \, dt \, \left| \int_0^{\infty} \chi_{\alpha\beta\gamma\delta}(t_1) \, |E_1(t-t_1)| \, dt_1 \right|^2 \quad (1)$$

where $\chi^{(3)}(t)$ is generally a fourth rank tensor with up to 81 nonvanishing elements.[24,25] In isotropic materials, however, only four elements need to be considered (i.e., χ_{zzzz}, χ_{yyzz}, χ_{yzyz}, χ_{zyyz}; here and throughout the paper we will consider experimental configurations in which the pulses are propagating along the x axis in the laboratory coordinate system as described in the Experimental Section).

The great advantage of ISRS in a grating geometry is its ability to project out certain single tensor elements of $\chi^{(3)}(t)$ simply by controlling the polarization states of the E fields that induce the third order response. $\chi^{(3)}(t)$ and, therefore, its elements contain distinct electronic and nuclear contributions. The former is instantaneous in time, meaning it is dominant during the duration of the pump pulses and negligible for delay times longer than the pulse duration. As was shown by Etchepare et al., the differences in symmetry properties allow for a suppression of the electronic response by adjusting the polarization conditions of the incoming fields and by proper selection of particular polarization components of the radiation emitted by the sample.[26] In general, TG-ISRS permits the direct and independent extraction of the modulus square of all four nonvanishing tensor elements of an isotropic material.

It should be noted, however, that the detection scheme of conventional TG-ISRS only allows for a measurement of $|\chi^{(3)}(t)|^2$ which should manifest itself in discrete sum and difference frequency (i.e., cross-) terms of individual Fourier components resulting from the impulsive excitation of fundamental Raman active modes. Furthermore, the modulus-square detection of TG-ISRS may affect and distort the overdamped response to $\chi^{(3)}$ which has been previously interpreted in terms of Kubo line shape theory to describe the dynamic nature of neat liquids.[17,27]

OHD-OKE, on the other hand, is basically a pump–probe polarization spectroscopy that was first implemented in the frequency domain by Eesley and Levenson[28] and transferred into the femtosecond time domain by Greene[15] and Kenney-Wallace and co-workers.[10] Optical heterodyning is achieved by providing a local oscillator field, E_{LO}, in addition to the signal field at the detector, resulting in much higher sensitivity and signal-to-noise ratio. If the optical phase of the local oscillator is well defined with respect to that of the probe field, the material response can be measured in a linearized form[23]

$$S_{\mathrm{OHD\text{-}OKE}}(t_d) \propto \int_{-\infty}^{\infty} E^*_{\mathrm{LO}}(t-t_d) \, E_2(t-t_d) \, dt \int_0^{\infty} \chi_{\alpha\beta\gamma\delta}(t_1) \, |E_1(t-t_1)|^2 \, dt_1 \quad (2)$$

thereby avoiding the appearance of cross-terms inherent to a modulus-square detection. If the local oscillator is in-quadrature with respect to the probe field, the signal becomes proportional to the real part of the material response, $\mathrm{Re}(\chi^{(3)}(t))$, representing the transient off-resonant birefringence, that is, the change in refractive index of the medium. By adjusting the local oscillator to be in-phase with the probe field, the imaginary part of $\chi^{(3)}(t)$ is measured and, therefore, the nonresonant transient dichroic response. Although OHD-OKE considers the complex nature of the third-order susceptibility explicitly, the major disadvantage of this experimental technique is its lack of ability to extract information about individual tensor elements of the response function. As a result, and in contrast to TG-ISRS, this method does not provide any elegant way to suppress either the electronic contribution or the nuclear contribution to $\chi^{(3)}(t)$.

The value of OHD-OKE as a probe for molecular dynamics of pure liquids has been shown in recent publications which explore the importance of solvent dynamics for ultrafast chemical reactions in solution.[18,23,29] The connection of solvation dynamics observed through time dependent fluorescence Stokes shift measurements and Kerr effect studies on the dynamics of the pure liquid has also been illustrated via a Brownian oscillator model and a frequency distribution of solvent modes (i.e., spectral density).[29] Cho, Fleming, and Mukamel have calculated the tensorial nonlinear response function of a chromophore exploiting the wave packet picture in Liouville space.[30] Furthermore, this model is also applicable to optical heterdyne detection and has been extended to off-resonant excitation as well.[23] More recently, Ziegler et al. have developed a theoretical description of resonant and nonresonant transient birefringence (as well as resonant and nonresonant transient dichroism) in terms of constructive and destructive interferences between different pathways in the time evolution of the density matrix.[31]

II. Experimental Section

The femtosecond laser system consists of a home-built Kerr lens mode locked Ti:sapphire laser pumped by the output of a CW argon ion laser (Coherent Innova 310) operating on all lines. The design of the x-folded Ti:sapphire oscillator follows closely the cavity described by Asaki et al.[32] A pump power of 5 W routinely yields a train of 15–20 fs duration pulses centered at 760 nm with a repetition rate of 85 MHz and 500 mW average power using a 10% output coupler at the nondispersive end of the resonator. Double passing the output beam through an extra-cavity fused silica prism arrangement compensates for the positive group velocity dispersion of the output coupler and the optics of the pump–probe interferometers that are described below.

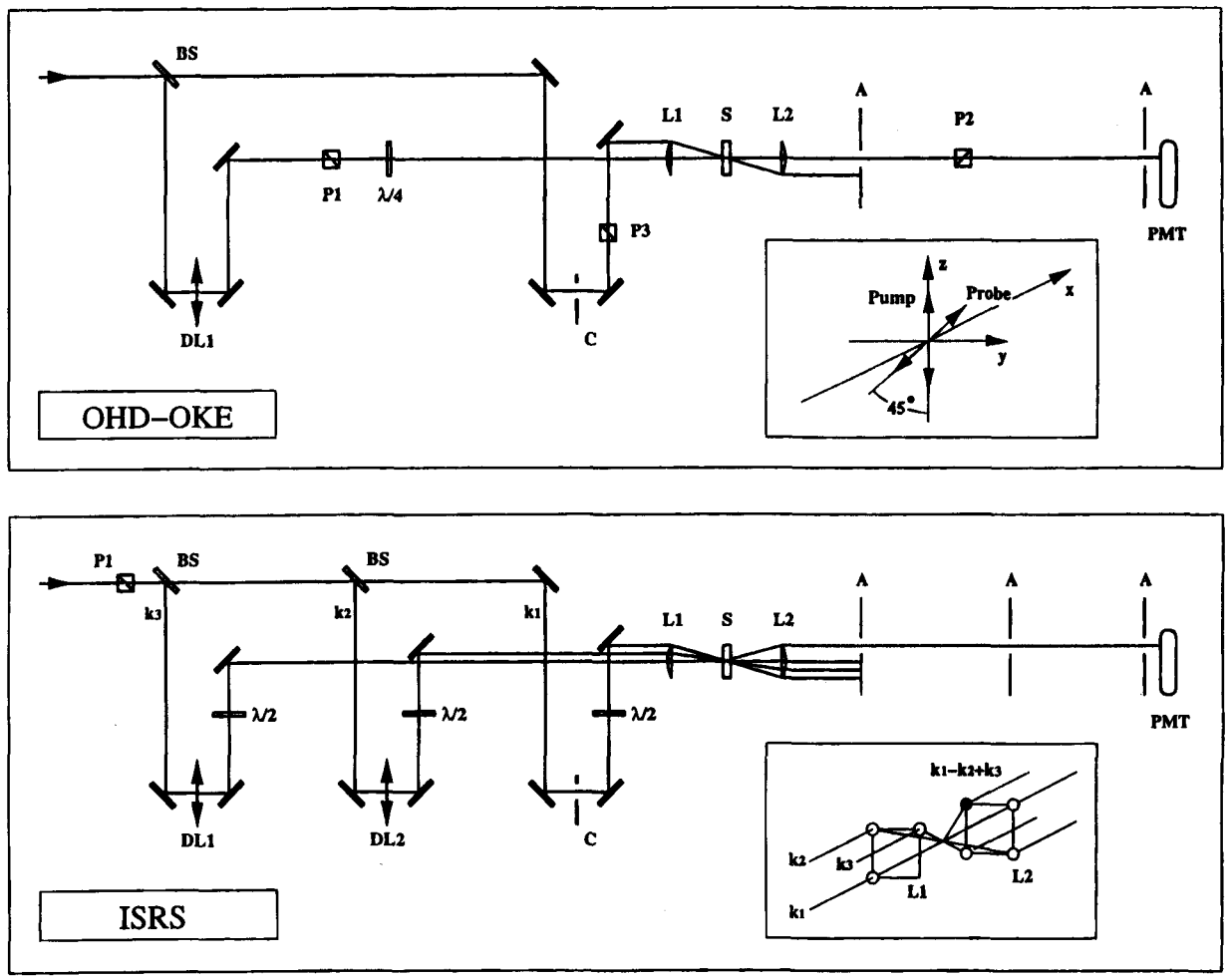

Figure 1. Experimental schematic for the OHD-OKE (upper panel) and TG-ISRS (lower panel) experiment: DL1 and DL2, optical delay lines; P1, P2, and P3, Glan-Taylor polarizers; BS, beam splitter; L1 and L2, achromatic lenses; L1 and L2, achromatic doublets; PMT, photomultiplier tube; A, aperture; $\lambda/2$, half-wave plate, $\lambda/4$, quarter-wave plate; C, optical chopper. The insets show the polarization conditions for the Kerr effect arrangement and the wavevector conditions in the BOXCAR geometry of the ISRS experiment.

OHD-OKE experiments were performed in a standard Kerr effect geometry[8,12,33] as shown in Figure 1. Probe pulses were derived from the original pulse train of the Ti:sapphire oscillator by using a surface reflection from an uncoated fused silica substrate; the remainder served as the pump beam. The probe beam delay with respect to the pump was controlled by a computer-driven translation stage (Nanomover, Melles Griot) with a maximum resolution of 0.33 fs/step. The probe beam passed through a pair of crossed Glan-Taylor polarizers (Karl Lambrecht Co.) that have a specified extinction of better than 10^5. The measured extinction of 2×10^6 was mainly limited by the static birefringence that arises from from the introduction of the special optical glass sample cell (Hellma, 1 mm optical path length) which could not be compensated by a zero-order quarter-wave plate (Mica, Karl-Lambrecht), which was located immediately after the entrance polarizer. The sample was carefully positioned in the pump and probe beams before each measurement to minimize leakage through the analyzer resulting from static birefringence and to reduce pump beam scatter. Pump and probe beams were focused into the sample and recollimated with 50.8 mm focal length achromatic doublets (Newport). The pump pulse polarization was adjusted to 45° with respect to the probe using a zero-order half-wave plate (CVI) and a Glan-Taylor polarizer (Karl Lambrecht Co). A $\pi/2$ local oscillator was derived by a slight rotation (<1°) of the quarter-wave plate oriented with its fast axis parallel to the polarization of the probe beam.

An alternative way to derive a local oscillator, which was avoided in the studies presented here, involves rotating the entrance polarizer rather than the quarter-wave plate[11]. This procedure results in an elliptically polarized probe beam with the long axis slightly tilted away from the axis of the entrance polarizer (i.e., tilted toward the axis of the analyzer). Therefore, this geometry creates polarization components that are both in-phase and out-of-phase with respect to the projection of the induced third-order response onto the transmission axis of the exit polarizer. (Note: the polarization of the LO with respect to the probe beam is not of relevance.) As a result, this particular geometry will yield a signal that is a mixture of nonresonant birefringence and nonresonant dichroism. In the limit of rotating the entrance polarizer by 45°, the probe beam emerging from the quarter-wave plate will be completely circularly polarized, and the third-order polarization transmitted by the analyzer would be heterodyned by both an in-phase and 90° out-of-phase local oscillator of equal amplitude. Hence, the resulting signal would be a 1:1 mixture of both the nonresonant birefringent and dichroic responses.

The pump-induced variation of the local oscillator was detected with an red- enhanced photomultiplier tube (Hamamatsu R928). Its output was directed to a digital lock-in amplifier (Stanford Research SR850) referenced to a chopper that modulated the pump beam at a frequency of 500 Hz. The transient birefringence was finally obtained by calculating the difference of two scans with local oscillator fields of equal amplitude but with an optical phase of opposite sign (i.e., $\pm\pi/2$).[34] The instrument response was determined as the pump–probe cross-correlation using background-free second harmonic generation in a 100 μm thick KDP crystal inserted at the position

of the sample cell. Each scan is composed of about 1000 data points with a step size of 4 fs.

The interferometer used in the transient grating ISRS experiments is shown in the lower part of Figure 1. Again the probe pulse was taken from a surface reflection from an uncoated fused silica substrate. A 50% reflector was used to split the remainder into two beams of equal intensity serving as the excitation pulses. The polarization of each beam could be adjusted independently with mica zero-order half-wave plates. The excitation and probe pulses were spatially overlapped and focused with 50 mm achromatic doublets ($f = 2$) in a standard BOXCAR geometry.[25] The beams were crossing in the fused silica sample cell at an angle of approximately 5°. The coherently scattered light in the wave vector direction $k_s = k_1 - k_2 - k_3$ (see inset in Figure 1) was recollimated with an achromat (Spindler & Hoyer, 80 mm focal length). Apertures were used to separate the signal field from the excitation and probe beams. The data collection and processing were done in the same way as described above. The temporal response was obtained by measuring the instantaneous ISRS response obtained from a 100 μm thick fused silica cover slip (ESCO). Again, a total number of 1000 data points were collected per scan with a step size of 4 fs. The samples were Fisher HPLC or spectral grade and used without further purification.

All data were analyzed by a program written in MATLAB (Wavemetrics) performing a linear prediction singular value decomposition (LP-SVD), which has proven to give more reliable results in analyzing such complex data as compared to commonly used nonlinear least squares fitting routines.[34,35] The LP-SVD method represents the signal as a sum of exponentially damped cosine functions,

$$S(t_d) = \sum_i A_i \, e^{-t_d/\tau_j} \cos(\omega_i t_d - \phi_i) \qquad (3)$$

Analysis yields the amplitudes A_i, frequencies ω_i, and damping constants τ_i as well as phase angles ϕ_i of all Fourier components that the signal is composed of. In general, the experimental data are fit from 40 fs onward to avoid any undesired interference from the electronic contribution that governs the response at early delay times. The precision of the phase angle depends on the frequency of the vibrational coherence and the accuracy of the zero time delay determined by measuring the pump−probe cross-correlation, which is estimated to be within 2 fs. The results of the LP-SVD analysis are summarized in Table 1.

III. Results

A. Optical Kerr Effect−Heterodyne Detection. The femtosecond-OHD-OKE transient for carbon tetrachloride with the nuclear contribution enlarged is shown in Figure 2. Transient birefringence measurements of carbon tetrachloride with 50−100 fs time resolution have been reported previously by Castner et al.,[18c] McMorrow et al.,[12] and Hattori et al.[14] Two modes with frequencies of 214 and 317 cm^{-1} are identified in the OHD-OKE signal and the LP-SVD analysis of CCl_4. The damping constants for both modes are about 1 ps, and the phase angles are close to 90°, indicating that both components appear as pure sine functions in the femtosecond transient. Their relative amplitudes are about 1:1.1. The wave form resulting from LP-SVD analysis is shown along with the experimental data (filled circles) in Figure 3; the fit is excellent.

The off-resonant transient birefringence response is given by eq 2 or, for the particular case of δ-shaped pulses and the

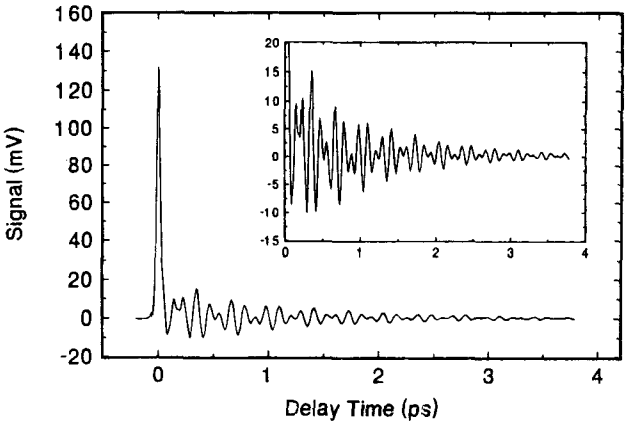

Figure 2. Experimental OHD-OKE transient for carbon tetrachloride. The inset shows a vertically expanded view of the nuclear dynamics.

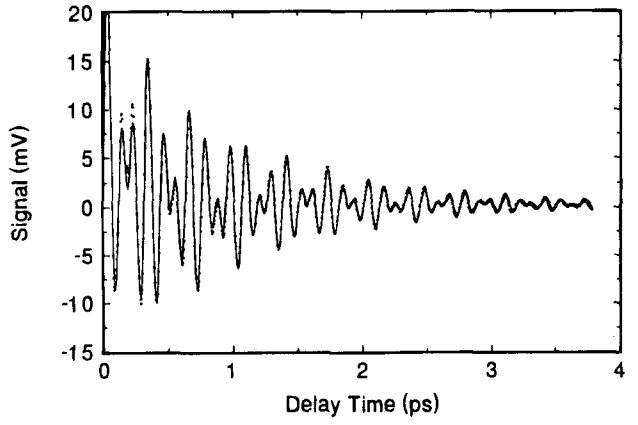

Figure 3. LP-SVD fit (solid curve) to the nuclear part of the transient birefringence data (solid circles) shown in Figure 2. The fit parameters are summarized in Table 2.

polarization conditions given in the Experimental Section, by

$$S^{\pi/2}_{\text{OHD-OKE}}(t_d) \propto \text{Re}[\chi_{zzzz}(t_d) - \chi_{yyzz}(t_d)] \qquad (4)$$

Following Hellwarth, the quantity in the brackets of eq 4 and the frequency domain analog thereof are denoted as the nonlinear optical response and the anisotropic part of the nonlinear optical susceptibility,[24] respectively. The frequency domain representation describes depolarized light scattering. Fourier transformation of eq 4 allows making a direct comparison to frequency domain data. The frequencies that we observe from LP- SVD analysis of the OHD-OKE data agree with the $\nu_2(0100)$ band at 218.7 cm^{-1} and the $\nu_4(0001)$ band at 316.3 cm^{-1} seen in the depolarized Raman spectrum reported by Schrader.[36] Moreover, the relative intensities of the modes are in excellent agreement with the values given in ref 36.

The transient birefringence data can also be represented in the frequency domain. However, since the measured signal is a convolution of the electronic and nuclear contributions to the third-order repsonse with the temporal profile of the pump pulse (cf. eq 2), deconvolution is required. The signal can be separated into the pure electronic contribution $\Delta\chi^e = (\chi^e_{zzzz} - \chi^e_{yyzz})$ and the pure nuclear contribution $\Delta\chi^n = (\chi^n_{zzzz} - \chi^n_{yyzz})$ to the material response by adopting the numerical procedure proposed in refs 11 and 23, which is a combination of a cubic spline with a fast Fourier transform algorithm. The electronic contribution is instantaneous in time and therefore simply follows the pump−probe pulse cross-correlation function, $I(t)$, which is measured independently. Taking into account the causality property of the response function allows eq 2 to be rewritten as

$$S_{\text{OHD-OKE}}(t_d) = \int_{-\infty}^{\infty} \Delta\chi^n I(t-t_d)\, dt + \Delta\chi^e I(t_d) \quad (5)$$

Hence, simple Fourier transformation of $S(t_d)$ and $I(t_d)$ yields the desired frequency representation of the nonlinear susceptibility according to[23]

$$\text{Im}[\chi^n_{zzzz}(\omega) - \chi^n_{yyzz}(\omega)] = \text{Im}\left(\frac{\mathcal{F}S(t_d)]}{\mathcal{F}I(t_d)]}\right) \quad (6)$$

and

$$\text{Re}[\chi^n_{zzzz}(\omega) - \chi^n_{yyzz}(\omega)] = \text{Re}\left(\frac{\mathcal{F}S(t_d)]}{\mathcal{F}I(t_d)]}\right) + [\chi^e_{zzzz}(\omega) - \chi^e_{yyzz}(\omega)] \quad (7)$$

It should be noted that the low-frequency range of eq 6 can be regarded as the distribution function of intermolecular equilibrium fluctuations of the liquid (i.e., the Raman spectral density) that contribute to the nuclear coordinate-dependent Raman polarizability.

Figure 4 presents the real and imaginary parts of the deconvoluted Fourier spectra of $\chi^{(3)}$. The large bandwidth of the laser (approximately 50 nm fwhm) and the superb signal-to-noise ratio of the OHD-OKE signal (approximately 50 000: 1) enables the observation of distinct spectral features well above 1000 cm^{-1}. In Figure 4 one can again identify the ν_2 and ν_4 modes as sharp peaks in Im[$\chi(\omega)$] around 214 and 318 cm^{-1} with relative intensities of 1:1.2. The slight asymmetric distortion of these peaks toward higher frequencies is presumably due to an artifact during the Fourier transformation and results from the finite accuracy (2 fs) in the zero time origin. The weak doublet structure around 770 cm^{-1} is known from frequency-domain Raman scattering to be due to a Fermi resonance between ν_3 and $\nu_1 + \nu_4$.[37] The doublet splitting is about 24 cm^{-1}. This value is well in excess of the spectral resolution of the scan, which is determined by the number of equally spaced time steps (1064) per total scan time (4 ps), in this case 0.24 THz or equivalently 8 cm^{-1}.

Finally, the frequency region between 0 and 200 cm^{-1}, which is the range not easily accessed by conventional depolarized light scattering, can be more precisely characterized here. The broad spectral band has a fwhm of approximately 60 cm^{-1} and is peaked at 25 cm^{-1}. It should be noted that these values are in good agreement with the far-IR spectrum calculated by Joslin and Gray[38a] as well as with the depolarized Rayleigh-wing spectrum reported by Lund et al.[38b] As mentioned earlier, this low-frequency distribution is exactly the spectral density that is necessary to describe the time scales of intermolecular motions and interactions of the liquid. These motions become apparent in OHD-OKE via a collision-induced term to the overall molecular polarizability that would otherwise be isotropic for spherical molecules, like CCl_4, and result in a vanishing depolarized component to the Raman signal.[39]

B. OKE–Homodyne Detection. Before turning to results obtained from the TG-ISRS experiments, it is useful to briefly consider the homodyne detected Kerr response of carbon tetrachloride. It represents a modulus-square detection of the nonlinear polarization, i.e., for δ-shaped pulses

$$S^{\text{homo}}_{\text{OHD-OKE}} \propto |\chi_{zzzz} - \chi_{yyzz}|^2 \quad (8)$$

The measured time domain data are shown in Figure 5. The relative intensities of homodyne-to-heterodyne signal depends upon the absolute pump pulse intensity but is also determined by the magnitude of the local oscillator employed in the latter measurement. The homodyne signal is typically at least an order of magnitude smaller than the heterodyne signal, even at the zero of time. The inset shows the same signal for delay times up to 2 ps and vertically expanded by a factor of 50. The most striking difference compared to the heterodyne detected signal is the relatively weak contribution from the nuclear dynamics. The magnitude of the first recurrence, barely seen in the unexpanded view of Figure 5, is just 1% of the electronic contribution. Furthermore, the nuclear Kerr response is dominated by an oscillatory component with a period of about 330 fs, corresponding to a vibrational coherence with a frequency of 100 cm^{-1}. Referring to eq 8, this quantum beat can be understood as resulting from a cross-term oscillating at the difference frequency of the ν_2 and ν_4 modes of CCl_4. This example shows that the intramolecular nuclear dynamics can be completely distorted by a modulus-square detection of the material response.

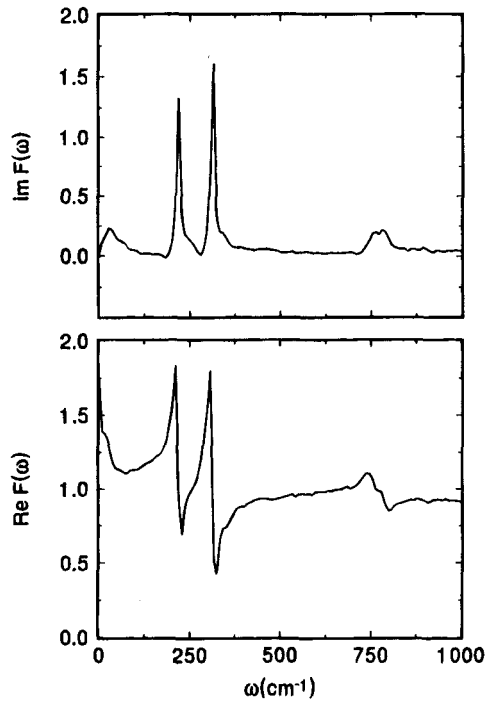

Figure 4. Imaginary and real parts of the deconvoluted Fourier transform $\chi(\omega)$ of the heterodyne detected Kerr response shown in Figure 2. Small amplitude oscillations and slight distortions of the peaks in the frequency spectrum result from finite scan length truncation and uncertainties in the zero time delay.

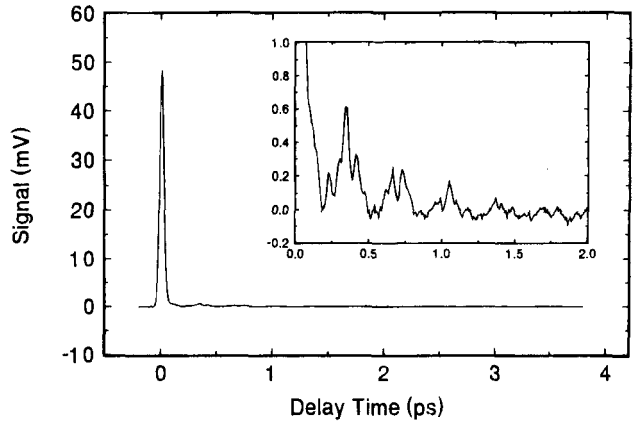

Figure 5. Homodyne detected transient birefringence of carbon tetrachloride. A vertically expanded view of the data is shown in the inset. The nuclear response is clearly dominated by a recurrence with a frequency of 100 cm^{-1}.

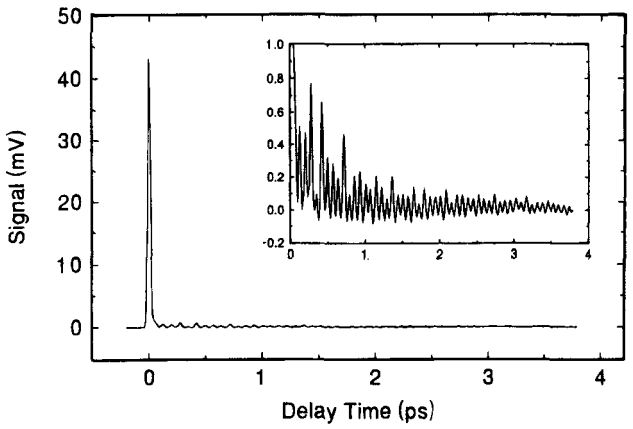

Figure 6. Transient grating optical heterodyne detected ISRS data of CCl_4 obtained with vertically polarized pump and probe pulses. The detected signal corresponds to $\chi_{zzzz}(t)$. A vertically expanded view of the nuclear contribution is shown in the inset.

TABLE 1: Parameters of the LP-SVD Fit to the Experimental Femtosecond Data Obtained in CCl_4

A (au)	ω (cm^{-1})	τ (ps)	ϕ (deg)
	(a) Transient Birefringence ($\chi_{zzzz} - \chi_{yyzz}$)		
5.01	313	1.03	−96
4.41	217	1.03	−88
5.04	0	0.30	0
	(b) TG-OHD-ISRS (χ_{zzzz})		
0.28	459	1.28	77
0.12	313	1.08	90
0.17	221	0.78	67
0.18	150	0.46	-33
0.38	0	0.43	0
	(c) TG-OHD-ISRS (χ_{yyzz})		
0.26	459	1.27	74
0.07	309	0.83	−70
0.08	212	0.77	−61
0.04	141	0.49	120
0.13	0	0.36	0
0.36	0	1.89	0
	(d) TG-OHD-ISRS ($\chi_{zzzz} - \chi_{yyzz}$)		
0.22	313	0.94	90
0.27	220	0.81	70
0.27	158	0.45	−62
0.41	0	0.06	0
0.04	0	1.31	0

To emphasize, it can be of crucial importance to pay attention to the complex nature of $P^{(3)}(t)$ when the focus of the study is to extract information about intermolecular dynamics of pure liquids from overdamped features in femtosecond ISRS data. Despite the large number of ISRS experiments on molecular dynamics of neat fluids, this aspect of the nonlinear polarization has not yet been considered.

C. Transient Grating OHD-ISRS in CCl_4. This subsection presents the results of transient grating optical heterodyne-detected ISRS experiments on CCl_4 with various polarization conditions for the pump and the probe pulses. Figure 6 shows a femtosecond transient obtained with pump and probe pulses polarized parallel with respect to each other and with respect to the **k** vector of the grating. This configuration is sensitive to χ_{zzzz}, which represents one of the tensor elements that constitutes the anisotropic component of the Raman response and, therefore, the transient birefringence signal . The nuclear dynamics are shown in detail in the inset of Figure 6. The results of the LP-SVD are listed in Table 1. As opposed to the transient birefringence, the signal is now governed by a vibrational coherence with a frequency of 459 cm^{-1}. This quantum beat matches very well with the totally symmetric ν_1 mode that is known from Raman spectra. The ν_1 mode exhibits a very low depolarization ratio of about 0.000 65,[40] which explains its absence in the OKE data. On the other hand, the ν_1 and ν_4 modes are characterized by depolarization ratios of approximately 0.9, consistent with their appearance in the transient birefringence and their (relatively) reduced intensities in the χ_{zzzz} measurement.

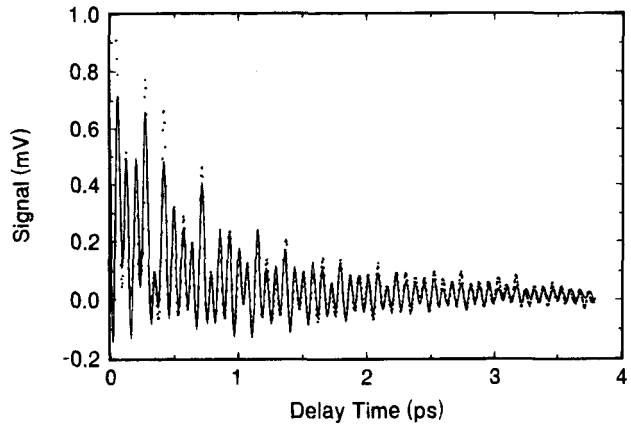

Figure 7. Experimentally determined nuclear contribution to $\chi_{zzzz}(t)$ (solid circles) of CCl_4. The solid curve represents an LP-SVD-fit to the data.The fit parameters are presented in Table 1.

The LP-SVD fit to the scattered signal is shown along with the experimental data in Figure 7. Apart from small deviations at early delay times, the overall quality of the fit is very good. The frequencies of the ν_2 and ν_4 modes agree, to within 2%, with the frequencies obtained from the OKE experiment. Their dephasing times are again close to 1 ps within an error of 20%. All intramolecular Raman-active modes give rise to negative sine functions in the TG-ISRS transient, as is evident from the phase angles being close to 90°. This observation indicates that the measured signal is heterodyne in nature with the local oscillator field $-\pi/2$ out-of-phase with respect to the signal field. Finally, the LP-SVD analysis reveals another oscillatory component at a frequency of 150 cm^{-1} that decays with a time constant of roughly 0.5 ps. Since this feature occurs at exactly the difference frequency of the ν_1 and ν_4 modes and since it decays twice as fast as the fundamentals, we conclude that some residual homodyne signal contaminates the "OHD-ISRS" response. Recall the detected signal results from the modulus-square detection of the sum of the electric fields incident on the detector. These fields include the local oscillator and the signal; hence, the detected signal contains the modulus square of E_{LO} and E_{Sig}, the latter of which constitutes the "homodyne" contamination, while the cross-term is proportional to E_{LO}. E_{Sig} constitutes the "heterodyne" response. To be clear, unlike the OHD-OKE measurement, TG-OHD-ISRS does not involve generation of a controlled local oscillator via polarization rotation and polarization analysis. In TG-OHD-ISRS the local oscillator derives directly from the sample. A more detailed discussion of this point is presented below.

The effect of imperfect heterodyning can be seen more clearly in the frequency domain representation. The deconvoluted Fourier spectra of the χ_{zzzz}-sensitive TG-ISRS experiment are shown in Figure 8. These spectra, as well as those to follow, have been calculated according to eqs 5−7 using the procedure described above. In accordance with the frequencies and phase angles obtained from the LP-SVD analysis, the imaginary part of the Fourier transform shows sharp negative peaks around 219, 316, and 457 cm^{-1}. Additional dispersive features in Im-$[\chi_{zzzz}(\omega)]$ can be seen in the spectral region around 149, 676, 773, and 913 cm^{-1} that precisely match the combination frequencies of $\nu_1 - \nu_2$, $\nu_1 + \nu_2$, $\nu_1 + \nu_4$, and $2\nu_1$, respectively.

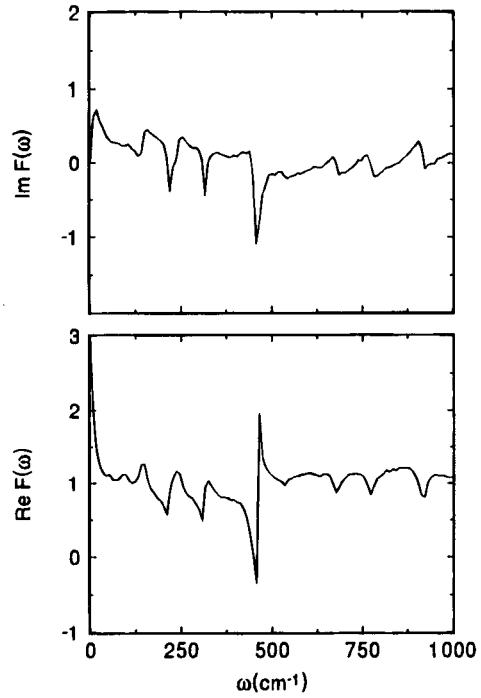

Figure 8. Imaginary and real parts of the deconvoluted Fourier spectrum $\chi_{zzzz}(\omega)$ obtained from the experimental femtosecond ISRS data shown in Figure 6.

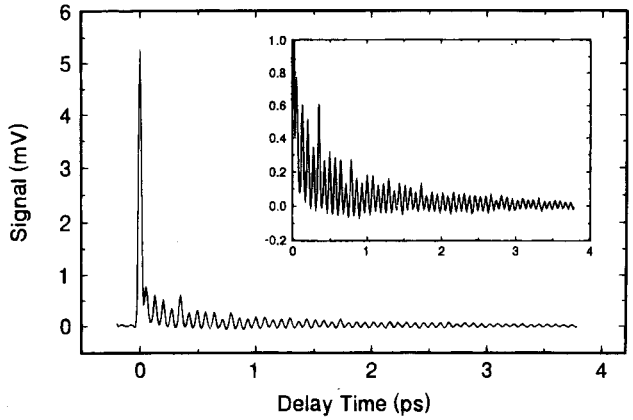

Figure 9. Transient grating optical heterodyne detected ISRS data of CCl_4 obtained with vertically polarized pump pulses and a horizontally polarized probe pulse. The detected signal corresponds to $\chi_{yyzz}(t)$. A vertically expanded view of the nuclear contribution is shown in the inset.

Finally, we point out that all coherences at combination frequencies appear as negative peaks in the real part of the Fourier transform. Therefore, these Fourier components are phase shifted by π with respect to the fundamentals. This phase shift is also characteristic of a modulus-square detection of oscillatory wave forms and, thus, supports the interpretation that a homodyne detected signal contributes to and slightly distorts the TG-OHD-ISRS transient.

Figure 9 presents the measurement of $\chi_{yyzz}(t)$ taken with both pump pulses polarized parallel with respect to the **k** vector of the transient grating and a perpendicular polarized probe pulse. At a first glance, both data sets look very similar in their nuclear response. However, there are slight differences in the envelope of the vibrational quantum beat pattern that are most clearly visible at delay times around 0.4 and 0.7 ps. Whenever a recurrence exhibits a maximum amplitude in $\chi_{zzzz}(t)$, a minimum is observed in $\chi_{yyzz}(t)$. The TG-ISRS data shown in Figures 6 and 9 have been collected back to back, without changing the overall alignment of the experiment, only rotating the 40 μm

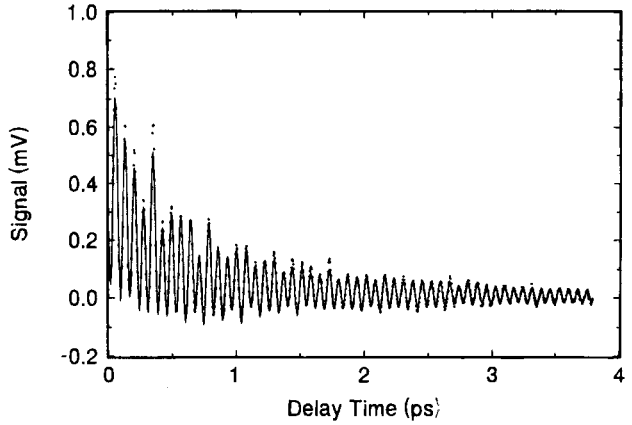

Figure 10. Experimentally determined nuclear contribution to $\chi_{yyzz}(t)$ (solid circles) of CCl_4. The solid curve represents an LP-SVD-fit to the data.The fit parameters are presented in Table 1.

thick half-wave plate in the probe beam arm of the pump–probe interferometer. This allows for making a direct comparison of the magnitudes of the electronic and nuclear response in both measurements. The amplitudes of the electronic responses in Figures 6 and 9 differ by a factor of 8.5. Since $\chi^e(t)$ at zero delay time in both experiments was much larger than any any background scatter, one can assume that the electronic response was completely homodyne detected. Therefore, we can conclude that the electronic part of χ_{zzzz} exceeds that of χ_{yyzz} by a factor of 2.9, in good agreement with the value of 3 implied by Kleinman symmetry,[24] which states that $\chi_{ZZZZ} = \chi_{YYZZ} + \chi_{YZYZ} + \chi_{YZZY}$. This agreement confirms that the measurements are in fact sensitive to the desired tensor elements. The amplitudes of the nuclear responses are given in Table 1.

Figure 10 shows the result of fitting the CCl_4 data to eq 3. Except for early delay times, the agreement between the LP-SVD fit and the experimental data is again very good. It is found that the amplitude of the ν_1 mode at 459 cm^{-1} is almost the same in both polarization configurations, while the magnitudes of the ν_2 and ν_4 modes (i.e., 215 and 310 cm^{-1}, respectively) are twice as large in the χ_{zzzz} data as in the χ_{yyzz} data. Again, within the accuracy of the experiment, the dephasing times for all vibrational coherences prepared agree very well with those obtained independently from the Kerr effect measurements shown in Figures 2–4 and the χ_{zzzz} data. Most importantly, however, a significant phase shift for the ν_2 and ν_4 modes of roughly 180° is found. In contrast, the totally symmetric mode ν_4 shows no phase shift at all. These differences are more clearly seen in the Fourier spectra shown in Figure 11. As was the case for $\chi_{zzzz}(\omega)$, both the real and the imaginary parts of the Fourier transform are clearly dominated by the ν_1 mode around 459 cm^{-1}, with a sharp negative peak in $\mathrm{Im}[\chi(\omega)]$ and a derivative-like feature in $\mathrm{Re}[\chi(\omega)]$. In the region of the ν_1 and ν_4 modes, the real part now shows positive peaks, which demonstrates conclusively the 180° phase shifts of these Fourier components with respect to $\chi_{zzzz}(\omega)$. As above, certain frequency components that are due to a nonnegligible homodyne contribution to the overall signal are observed, particularly at the frequency of the second harmonic of the ν_1 band.

D. OHD-OKE and TG-OHD-ISRS in Benzene. The heterodyne detected TG-ISRS signal has been observed in other liquids including $CHCl_3$ and benzene. For brevity, we will focus on the benzene transients to further illustrate the competition between OHD and modulus-square contributions to ISRS in transient grating geometries. The observations for benzene are generally the same as for CCl_4, but the larger molecular polarizibility and dominant intermolecular contribution to the

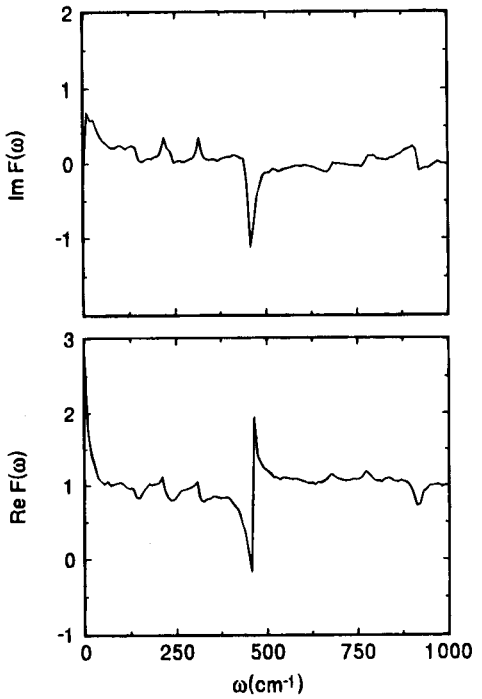

Figure 11. Imaginary and real parts of the deconvoluted Fourier spectrum $\chi_{yyzz}(\omega)$ obtained from the experimental femtosecond-ISRS data shown in Figure 9.

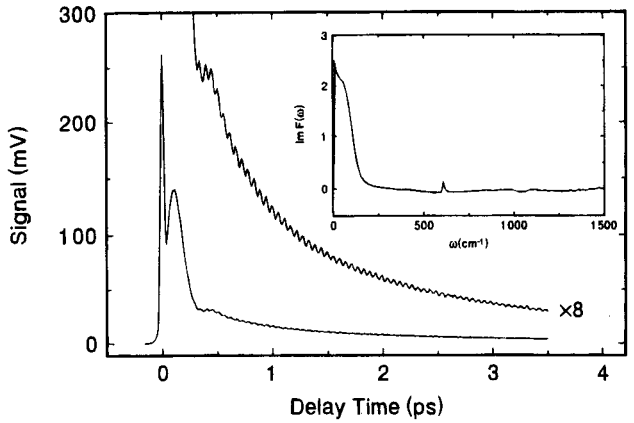

Figure 12. Experimental OHD-OKE transient obtained for benzene. The inset shows the imaginary part of the deconvoluted Fourier transform of the time domain data.

signal provide a clear comparison of signals resulting from the product of different dynamical responses (i.e., cross-terms from modulus-square detection) as opposed to heterodyne detection.

The OHD-OKE transient response of benzene is shown in Figure 12. LP-SVD analysis reveals two modes, one with a frequency of 88 cm^{-1} and the other at 608 cm^{-1}. The low-frequency oscillation corresponds to a collection of underdamped intermolecular modes that behave as one nearly critically damped oscillator. The high-frequency mode is the depolarized ν_{18} intramolecular C−C in-plane bending motion.[41,42] The inset in Figure 12 shows the imaginary part of the deconvoluted Fourier transform of the time domain data. This curve is dominated by the low-frequency amplitude which is in good agreement with previous OHD-OKE results;[43] the higher frequency region has not been reported before. It should be noted that the anisotropic (D_{6h}) nature of benzene, as opposed to the T_d symmetric form for CCl_4, allows for a slowly decaying contribution to the nonlinear optical repsonse,[43,44] reflecting orientational diffusion of benzene. The homodyne signal measured in the OKE geometry and Fourier transform, both not displayed, show a significantly reduced nuclear (vs elec-

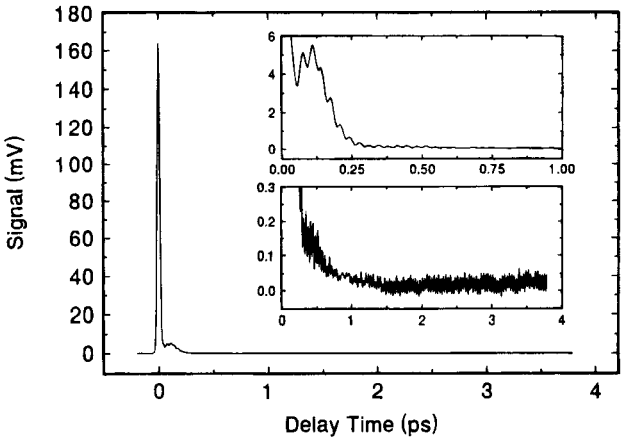

Figure 13. Impulsive stimulated Raman scattering data of benzene obtained in a transient grating geometry with vertically polarized pump pulses and a vertically polarized probe pulse. The insets show enlarged portions of the nuclear contribution to the signal.

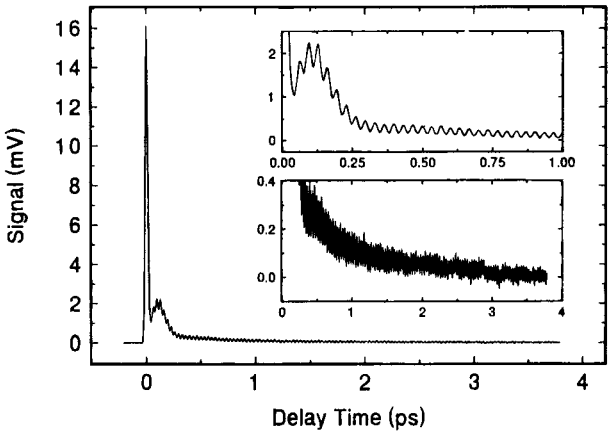

Figure 14. Impulsive stimulated Raman scattering data of benzene obtained in a transient grating geometry with vertically polarized pump pulses and a horizontally polarized probe pulse. The insets show enlarged portions of the nuclear contribution to the signal.

tronic) amplitude but with a residual component at 608 cm^{-1}. This component arises as a cross-term between the low-frequency intermolecular motions and the intramolecular mode.[45]

The transient grating ISRS responses in benzene for parallel and perpendicular polarizations, selecting χ_{zzzz} and χ_{yyzz}, are shown in Figures 13 and 14. The $t = 0$ responses are in a ratio of 10:1 as expected from Kleinman symmetry and modulus-square detection. Expanded views are presented in the insets. Comparison of the parallel and perpendicular results shows an oscillation with the same frequency in both but initially of opposite phase. The oscillation in the parallel data damp out near 0.9 ps delay and re-form with the same phase as the perpendicular. The frequency of the oscillation in the parallel and perpendicular data, obtained by LP-SVD analysis, is 992 cm^{-1}, corresponding to the strongly polarized symmetric ring breathing mode. The LP-SVD fit parameters for the OKE and ISRS data are given in Table 2.

Figure 15 shows the imaginary parts of the deconvoluted Fourier transforms of the parallel (upper panel) and perpendicular transients (lower panel). Along with the phase angle results given in Table 2, the frequency domain representation of the benzene data show the 180° phase shift for the polarized mode at early times. This result is in agreement with the observations for the depolarized modes in CCl_4. The parallel and perpendicular scans do, however, have the same phase at later times, in agreement with the experimental results on the polarized mode of CCl_4 described earlier. While the perpen-

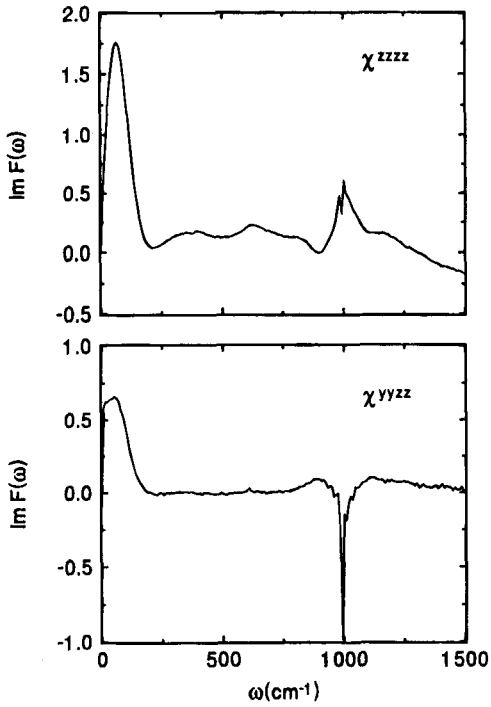

Figure 15. Imaginary parts of the deconvoluted Fourier transforms of the TG-ISRS data of benzene. The upper curve corresponds to data displayed in Figure 13. The lower trace shows the deconvoluted Fourier spectrum of the data shown in Figure 14.

TABLE 2: Parameters of the LP-SVD Fit to the Experimental Femtosecond Data Obtained in Benzene

A (au)	ω (cm^{-1})	τ (ps)	ϕ (deg)
	(a) Transient Birefringence		
0.59	607	1.37	−93
121.4	88	0.10	−152
107.7	0	0.02	0
107.1	0	0.13	0
32.7	0	0.56	0
14.5	0	2.53	0
	(b) TG-OHD-ISRS (χ_{zzzz})		
0.004	992	−3.20	−308
0.58	966	0.13	−90
6.43	131	0.07	−228
18.9	0	0.07	0
0.07	0	1.75	0
	(c) TG-OHD-ISRS (χ_{yyzz})		
0.03	992	0.36	−247
0.12	989	7.42	−267
1.40	94	0.10	−146
1.94	0	0.14	0
0.27	0	1.16	0

dicular data for the intramolecular mode of benzene is completely heterodyne in nature, the parallel transient is mostly homodyne detected at early delay times and completely heterodyne detected at delay times larger than 1 ps. At a delay time of about 0.9 ps, the magnitude of the local oscillator derived from the additional scattering response of the sample (see below) is comparable to that of the signal itself, resulting in a π-phase shift in the oscillatory modulation at 992 cm^{-1} and yielding a node at that particular time delay. This node structure resembles a beat pattern arising from two oscillatory components with a difference frequency of 1/0.9 ps^{-1} centered at 992 cm^{-1}. This splitting can be clearly seen in the imaginary part of the deconvoluted Fourier spectrum (see upper panel in Figure 15). Since we do not observe any node structure in the χ_{yyzz} data, the additional diffracted field that causes heterodyning seems to be more efficiently produced for light polarized parallel to the **k** vector of the grating than for light polarized perpendicular. Hence, the magnitude of the local oscillator in the χ_{yyzz} data was larger than scattering resulting from the ISRS excitation at any given time delay. This source of the heterodyning, i.e., local oscillator, field is discussed below.

The critically damped low-frequency feature and the slowly decaying exponential background that are seen in all benzene data deserve further attention. The Fourier component around 100 cm^{-1} appears with the same frequency, phase angle, and time constant in both the OHD-OKE and the perpendicular data. Again, this indicates that these scattering data are mostly heterodyne detected. (A small homodyne contribution to the perpendicular data can be identified with a very rapidly decaying modulation at 992 cm^{-1}.) On the other hand, the low-frequency component shows a significantly reduced time constant in the parallel data and a frequency (ω = 131 cm^{-1}) about 50% larger compared to both the perpendicular transient and the OHD-OKE responses. Since this feature dominates the nuclear response at early times (<1ps), the observations and fitted parameters can be attributed to the greater homodyne character of the parallel data. Furthermore, the single exponential decay constant (τ = 1.16 ps), reflecting orientational diffusion of benzene, is about a factor of 1.5 smaller than in the perpendicular data and twice as fast as that obtained from the Kerr response. These observations are again in agreement with the homodyne character of the transient scattering response obtained with parallel polarized pump and probe pulses.

The LP-SVD analysis, which is summarized in Table 2, taken together with the interpretation given above, clearly shows that the intermolecular dynamics can be distorted by modulus-square detection. Since there is no unambiguous method to extract the linearized response from the homodyne detected signal, the results presented here demonstrate that optical heterodyne detection in any off-resonant time domain Raman experiment is obligatory for obtaining reliable information about dynamics in pure liquids.

IV. Discussion

A. Local Oscillator in the Scattering Geometry. The results and analysis presented above clearly indicate that the measured signals are partially or completely heterodyne in nature. This is demonstrated through a careful analysis and comparison of the phase angle and frequency of the intramolecular modes that contribute to the OKE and transient grating ISRS signals. The demonstrated heterodyne nature of our TG-ISRS signal for these two simple liquids is also made manifest by consideration of the symmetry of the molecule and the symmetric or nonsymmetric nature of the particular vibrational motions. Here we further describe the nature and source of the local oscillator field.

The local oscillator field for the scattered signal has a well defined and constant relative optical phase with respect to that of the diffracted probe field; the latter resulting from the prompt polarization response $P^{(3)}(t)$. Sensitivity to optical phase requires that this local oscillator field be obtained from the probe beam and that it is not a simple reflection of the k_1 and k_2 pump beams from the sample cell. The measured TG-ISRS response of a 0.1 mm thick piece of fused silica and the TG-ISRS responses of the entrance and exit faces of our sample cell yield the pump−probe cross-correlation, indicating that the third-order response of fused silica is instantaneous in time. Hence, optical heterodyning from light scattering from the sample cell windows can only occur near zero time delay but not at the longer delay times that are relevant to the nuclear responses. This heterodyning mechanism can, however, be of importance if the signal

is detected forward direction, as is the case for OKE and ordinary pump−probe measurements. The only possible source for the local oscillator field is another diffraction source such as that resulting from a sample grating with the same fringe pattern as the grating associated with the femtosecond-to-picosecond polarization.

The high average power delivered to the sample in the pump and probe beams (approximately 300 mW) is capable of inducing thermal gratings.[46] Since the sample is not flowing, the accumulated thermal, i.e., phase, grating is only dissipated by thermal diffusion, resulting in dissipation times on the order of microseconds. The probe beam scatter off of this accumulated phase grating is toward the detector and along the same **k** vector direction as the scattering (i.e., diffraction) that results from the prompt (femtosecond to picosecond) polarization response of the sample. In particular, the probe light scattered from the thermal grating is a constant background, which is independent of the pump−probe delay on a picosecond time scale, and has a phase shift of 90°.[46] This thermal scattered field serves as an in-quadrature local oscillator, resulting in a portion of the total (polarization) signal to be heterodyne detected. Therefore, the real part of the nonlinear optical response function is measured. The relative magnitude of this thermally scattered electric field compared with the scattering from the instantaneous polarization determines the degree to which the detected signal is purely linearized, mixed heterodyne/homodyne, or purely homodyne in nature.

B. Comparison of OHD-OKE with TG-OHD-ISRS. According to eq 8, the time-resolved transient birefringence response of carbon tetrachloride presented in section IIIA, is a linear combination of two individual tensor elements. The analysis of the transient grating ISRS data of CCl_4 demonstrated the independent determination of these tensor components via optical heterodyne detection in an impulsive stimulated scattering geometry. The reliability of the TG-OHD-ISRS results may be tested by reconstructing the birefringent response from the data shown in Figures 6 and 9 and comparing these results with the experimental data obtained in the Kerr effect geometry. This must be done with consideration that the local oscillator field employed in the TG-ISRS detection scheme has been $-\pi/2$ out of phase with respect to the third-order polarization; i.e., all Fourier components appear as minus-sine-functions in the χ_{zzzz} data. Therefore, the experimental results depicted in Figures 6 and 9 actually represent the quantities $-\chi_{zzzz}$ and $-\chi_{yyzz}$. Simple subtraction of these femtosecond ISRS transients with consideration of their sign yields the upper curve in Figure 16. For comparison, the experimental transient birefringence data are shown as the lower trace in Figure 16. Because the electronic response is an instantaneous function in time, and since χ^e was purely homodyne detected, only the nuclear contributions to the third order response are displayed. Apart from small deviations at early delay times, the agreement is very good. This close agreement not only proves the consistency of the OHD-ISRS data but also demonstrates the capability of this technique to simultaneously determine both the isotropic (χ_{yyzz}) and anisotropic ($\chi_{zzzz} - \chi_{yyzz}$) parts of the nonlinear susceptibility, the components that are responsible for polarized and depolarized light scattering, respectively.

This result is of particular significance in the low-frequency range, i.e., below 200 cm^{-1}. In general, the technique of optical heterodyning the various tensor elements of $\chi^{(3)}$ allows, in a unique way, for a full description of the spectral density of collective intermolecular liquid modes that contribute to both polarized and depolarized inelastic scattering. In that sense, OHD-ISRS in a grating geometry can give a more complete

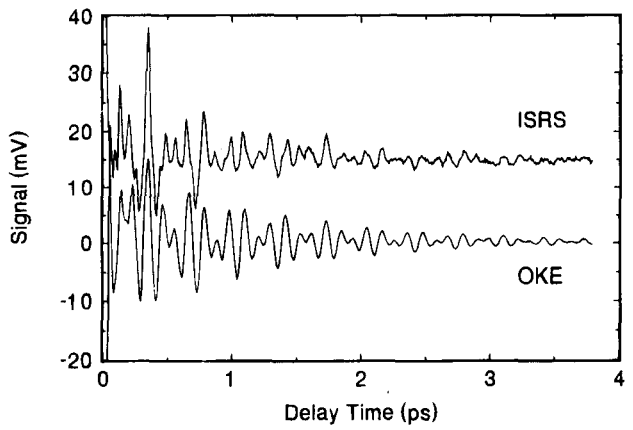

Figure 16. Comparison of the nuclear contribution to $\chi_{zzzz}(t) - \chi_{yyzz}(t)$ of carbon tetrachloride obtained from transient birefringence and TG-OHD-ISRS measurements. The upper curve was constructed by computing the difference between the data shown in Figures 6 and 9.

and detailed insight into the time scale of equilibrium fluctuations of the liquid than, for example, OHD-OKE, because of the insensitivity of the latter technique to polarized intermolecular solvent degrees of freedom. The concept of using transient birefringence data as a measure of the frequency dependence of the solvent fluctuations that couple the liquid to a solute chromophore has successfully been used in the description of the solvation correlation function of a Coumarin dye in acetonitrile.[29] Recently, OHD-OKE data have become extremely important in correlating the dynamics of optical dephasing processes to the spectral density of the pure solvent for a weakly interacting cyanine dye chromophore molecule.[4] This approach should be applicable to strongly interacting solutes, too, taking the frequency dependence of the coupling strength into account. Similarly, the importance of solvent fluctuations that can couple to a reaction coordinate, such as in electron-transfer processes, should be emphasized. The relative magnitude of the spectral density has also been shown to explain the rate of iodine B-state predissociations in *n*-alkane solutions.[47]

The isotropic and anisotropic Raman low-frequency spectral densities seen in the data for CCl_4 and benzene are different. However, the incomplete heterodyning of these signals due to a local oscillator field of insufficient amplitude also causes a distortion of the low frequency spectra which is not easily quantified through a phase angle analysis. We hope to reduce the issue with a controllable local oscillator using phase-locking methods (see Section IVD).

C. Phase of Intramolecular Vibrations. It was noticed that the phase angles for the totally symmetric mode of carbon tetrachloride (cf. 460 cm^{-1}) displayed in Figures 6 and 9 are exactly identical in both measurements. Consequently, this mode will not appear in the anisotropic part of the nonlinear susceptibility, nor in the transient birefringence, if the amplitudes of the corresponding modulations in both contributing tensor components of $\chi^{(3)}(t)$ are exactly identical (cf. eq 4). Alternatively, this mode will be characterized by a depolarization ratio close to zero and will only appear in the polarized light scattering spectrum. The fact that the same phase angle is detected in both polarization configuration is due to the A_1 symmetry of this mode: synchronous stretching of all four C−Cl bonds. The periodic change of the collective polarizability at the particular frequency of the ν_1 mode, induced by impulsive and coherent excitation of that mode by two *z*-polarized pump pulses, will be isotropic with respect to the laboratory frame. The projection of this periodic change in polarizability onto the *z* and *y* axes will be equal for all pump−probe time delays. As a result, the Fourier component of the scattered signal for both polarization

configurations (χ_{zzzz} and χ_{yyzz}) will have the same amplitude and will be exactly in phase with each other.

In contrast, the ν_2 and ν_4 modes of carbon tetrachloride at 217 and 312 cm^{-1} have E and T_2 symmetry, respectively. Impulsive and coherent excitation of these deformation modes also results in a periodic change in polarizability which is now anisotropic with respect to the molecular and laboratory frames. The projections of the molecular polarizability onto the z and y axes will exhibit the same frequency but, due to the symmetry of these vibrations, have different amplitudes and oscillate 180° phase shifted with respect to each other. Therefore, the χ_{zzzz} transient, which is sensitive to the projection onto the z axis defined by the pump pulses, and the χ_{yyzz} transient, which probes a projection orthogonal to the pump pulses and orthogonal to the **k** vector of the probe pulse, are expected to display sinusoidal modulations with the same frequency but π-phase-shifted and of different amplitude. This is precisely what was observed.

In analyzing the scattering results of benzene described in section IIID, it was noticed that the Fourier components at 992 cm^{-1} observed in the parallel and perpendicular polarization configurations have exactly opposite phases. However, since the parallel data are mostly homodyne detected at early times, one has to compare the phase angles at delay times larger than 1 ps. In fact, a close inspection of the two ISRS transients at large delay times (>1 ps) shows that the oscillations at 992 cm^{-1} are perfectly in-phase with each other. Again, this can be attributed to the symmetric nature of the ring breathing mode of benzene (symmetry A_{1g}), which gives rise to a modulation of $\chi^{(3)}(t)$ that is isotropic with respect to the laboratory frame, in agreement with results obtained from the totally symmetric ν_1 mode of carbon tetrachloride.

D. Phase-Locked OHD-ISRS. It was noticed that the Fourier transforms of the ISRS signal exhibit features that are due to incomplete heterodyning of the third order response of the sample. Recently, Scherer et al.[20] have experimentally demonstrated the control of the relative phases of femtosecond duration optical pulses for time delays that are much longer than the actual pulse widths. The transient grating impulsive stimulated Raman scattering experiment could be extended to a configuration that involves a four-pulse, pump−probe LO sequence. The fourth pulse is intended to interfere with the third-order polarization at the position of the detector. To detect the nonresonant material response in a linearized form, it is essential to have precise control of the relative phase of the fourth E field, which represents the local oscillator field, and the third field, which is to be scattered off the transient grating induced by the first two pump pulses. Moreover, by adjusting the local oscillator to be in-phase or in-quadrature with the third field should allow selectively obtaining the real and imaginary parts of the third-order nonlinear optical response. The Kramers−Kronig relationships were implicitly used in the Fourier transform analysis presented in section III to determine the real and imaginary parts of $\chi^{(3)}$. In this sense, this phase-locking approach represents the complete nonresonant equivalent to the heterodyne detected stimulated photon echo (HSPD) experiment, recently proposed by Cho et al.[48] to elucidate the real and imaginary parts of the nonlinear response function of a resonant chromophore. The major advantage of using phase locked optical pulses over the experiment described in this paper is that the former technique allows for the adjustment of the relative magnitude of the local oscillator field to be orders of magnitude larger than the signal field itself, thereby ensuring the comparative suppression of any residual homodyne contribution.

Preliminary phase related pulse OHD-ISRS measurements have been undertaken that show the effect of changing the local oscillator phase on the heterodyne detected ISRS response[49]. These results and the experimental scheme will be reported elsewhere.

V. Summary and Conclusions

In conclusion, we have described the experimental determination of the off-resonant nonlinear third-order response of a simple liquid, carbon tetrachloride, by optical heterodyne detected stimulated Raman scattering. This polarization sensitive transient grating technique allows direct and independent measurements of the real and imaginary parts of individual elements of the fourth-rank tensor $\chi^{(3)}$. This approach combines the advantages of conventional transient grating ISRS with those of optical heterodyne detected Raman induced Kerr effect spectroscopy.

The justification for this interpretation of the measured TG-ISRS responses is made possible through the high quality of the data, allowing a direct comparison of the scattering data to OHD-OKE measurements. It was shown that intramolecular Raman-active vibrations give rise to oscillatory modulations of the linearly detected third-order response whose phase angles are defined by the symmetry of those modes. In particular, it was observed that the amplitudes and phase angles of vibrational coherences corresponding to completely polarized modes are independent of the particular polarization of the probe beam and are, therefore, the same for all tensor elements that compose the anisotropic part of the nonlinear susceptibility. For modes that exhibit a high depolarization ratio in frequency domain light scattering, a 90° phase shift of corresponding Fourier components of these tensor elements was found. The enhanced capability of this technique to characterize the low-frequency distribution of liquid modes that give rise to both polarized and depolarized light scattering was discussed.

Transient grating OHD-ISRS, therefore, permits a more complete description of the solvent spectral density that can be used to quantify equilibrium fluctuations in neat liquids. The results of such studies can be used to accurately quantify interactions of chromophores with their surrounding solvent bath as well as to compare and predict chemical reaction dynamics, such as dissociation, isomerization, or electron-transfer processes in condensed media. Recently, the connection between dynamics of electronic dephasing observed through degenerate four-wave mixing studies and the spectral density of solvent states has successfully been made by predicting the two-pulse photon echo decays of various dye molecules from experimentally determined solvent spectral densities (i.e., Fourier transforms of birefringence responses) for a variety of solvents.[4] Moreover, the dynamics of the photoinduced dissociation of iodine in the B state could be correlated surprisingly well with the spectral density of the solvent for the homologous series of n- alkanes.[47] These two independent studies exemplify how a better microscopic understanding of chemical processes in the liquid phase can be provided by a more precise description of the dynamics of neat liquids as obtained from time resolved femtosecond Raman spectroscopies.

Finally, we have proposed the application of phase-locked optical pulses in an impulsive stimulated Raman scattering arrangement, thereby providing a local oscillator that is controlled with respect to its amplitude and its phase in a very simple and elegant way. This method has the advantage of being able to unravel the pure linearized response from the homodyne background. The implementation of optical pump−probe techniques involving phase-locked femtosecond optical

pulses is currently in progress in our laboratory, and their application to resonant and nonresonant interactions will be the topic of a forthcoming paper. The application of phase-locked optical pulses to the detection of higher-order nonlinearities such as $\chi^{(5)}$ and $\chi^{(7)}$ seems obvious. Those formal extensions of the method described here should be able to provide detailed insight into the homogeneous and inhomogeneous nature of the spectral density that one obtains from third-order techniques such as OHD-OKE and TG-OHD-ISRS.

Acknowledgment. Stuart Rice is and has been an inspiration and a mentor to a large number of physical chemists. I consider myself fortunate to be in this company. I thank Stuart for his excellent teaching in the classroom and in our common research. Our paths have crossed many times but mostly in a nonchaotic fashion. We thank Professor S. Ruhman for helpful discussions during his visit to the University of Pennsylvania. We also thank the reviewer for a very careful reading of the manuscript and making many useful comments. We thank the Deutsche Forschungsgemeinschaft for fellowship support and the National Science Foundation for a National Young Investigator Award. This research was partially supported by a grant from the Petroleum Research Fund of the Americal Chemical Society. We acknowledge the National Science Foundation for equipment support through Grant CHE92-21000 and support of the University of Pennsylvania Materials Research Lab through NSF Grant DMR91-20668. N.F.S. is a recipient of a David and Lucille Packard Foundation Fellowship.

References and Notes

(1) See for example: (a) Schroeder, J. ; Troe, J. *Annu. Rev. Phys. Chem.* **1987**, *38*, 136. (b) Schroeder, J.; Troe, J.; Vöhringer, P. *Chem. Phys. Lett.* **1993**, *203*, 255.

(2) See for example: (a) Barbara, P. F.; Jarzeba, W. *Adv. Photochem.* **1990**, *15*, 6. (b) Fleming, G. R.; Wolynes, P. G. *Phys. Today* May **1990**, (May), 41.

(3) Haynes, G. R.; Voth, G. A. *J. Chem. Phys.* **1993**, *99*, 8005.

(4) Vöhringer, P.; Arnett, D. C.; Westervelt, R. A.; Feldstein, M. J.; Scherer, N. F. *J. Chem. Phys.*, submitted.

(5) (a) Yan, Y.-X.; Cheng, L.-T.; Nelson, K. A. In *Advances in Non-Linear Spectroscopy*; Clark, R. J. H., Hester, R. E., Eds.; John Wiley and Sons: New York, 1990. (b) Nelson, K. A.; Ippen, E. P. *Annu. Rev. Phys. Chem.* (c) Fayer, M. D. *Ibid.* **1982**, *33*, 63.

(6) (a) Ruhman, S.; Joly, A. G.; Nelson, K. A. *J. Chem. Phys.* **1987**, *86*, 6563. (b) Ruhman, S.; Kohler, B.; Joly, A. G.; Nelson, K. A. *IEEE J. Quantum Electron.* **1988**, *QE-24*, 460. (c) Ruhman, S.; Joly, A. G.; Kohler, B.; Williams, L. R.; Nelson, K. A. *Rev. Phys. Appl.* **1987**, *22*, 1717.

(7) (a) Yan, Y.-X.; Nelson, K. A. *J. Chem. Phys.* **1987**, *87*, 6240. (b) *Ibid.* **1987**, *87*, 6257. (c) Yan, Y.-X.; Gamble, Jr., E. B.; Nelson, K. A. *J. Chem. Phys.* **1985**, *83*, 5391.

(8) (a) Ruhman, S.; Williams, L. R.; Joly, A. G.; Kohler, B.; Nelson, K. A. *J. Phys. Chem.* **1987**, *91*, 2237. (b) Ruhman, S.; Kohler, B.; Joly, A. G.; Nelson, K. A. *IEEE J. Quantum Electron.* **1988**, *QE-24*, 470.

(9) Ippen, E. P.; Shank, C. V. *Appl. Phys. Lett.* **1975**, *26*, 92.

(10) (a) Kalpouzos, C.; Lotshaw, W. T.; McMorrow, D.; Kenny-Wallace, G. A. *J. Phys. Chem.* **1987**, *91*, 2082. (b) Lotshaw, W. T.; McMorrow, D.; Kalpouzos, C.; Kenny-Wallace, G. A. *Chem. Phys. Lett.* **1987**, *136*, 323.

(11) (a) McMorrow, D.; Lotshaw, W. T. *J. Phys. Chem.* **1991**, *95*, 10359. (b) McMorrow, D.; Lotshaw, W. T. *Chem. Phys. Lett.* **1990**, *174*, 85.

(12) Lotshaw, W. T.; McMorrow, D.; Kenny-Wallace, G. A. *IEEE J. Quantum Electron.* **1988**, *QE-24*, 443.

(13) Kobayashi, T. *Adv. Phys. Chem.* **1994**, *85*, 55.

(14) Hattori, T.; Kobayashi, T. *J. Chem. Phys.* **1992**, *94*, 3332.

(15) (a) Greene, B. I.; Farrow, R. C. *Chem. Phys. Lett.* **1983**, *98*, 273. (b) Greene, B. I.; Fleury, P. A.; Carter, H. L.; Farrow, R. C. *Phys. Rev. A* **1984**, *92*, 271.

(16) (a) Berne, B. J.; Pecora, R. *Dynamic Light Scattering*; John Wiley & Sons: New York, 1990. (b) Rothchild, W. G. *Dynamics of Molecular Liquids*; John Wiley & Sons: New York, 1984.

(17) Ruhman, S., Nelson, K. A. *J. Chem. Phys.* **1991**, *94*, 859

(18) (a) Chang, Y. J.; Castner, Jr., E. W. *J. Chem. Phys.* **1993**, *99*, 113. (b) *Ibid.* **1993**, *99*, 7289. (c) Castner, Jr., E. W.; Chang, Y. J., Melinger, McMorrow, D. *J. Lumin.* **1994**, *60, 61*, 723.

(19) (a) Gordon, R. G. *J. Chem. Phys.* **1965**, *43*, 1307. (b) Madden, P. A.; Tildesley, D. J. *Mol. Phys.* **1985**, *55*, 969. (c) *Ibid.* **1983**, *48*, 129. (c) Steele, W. A. *Adv. Chem. Phys.* **1976**, *53*, 1.

(20) (a) Scherer, N. F.; Ruggiero, A.; Du, M.; Fleming, G. R. *J. Chem. Phys.* **1990**, *93*, 856. (b) Scherer, N. F.; Carlson, R. J.; Matro, A.; Du, M.; Ruggiero, A.; Romero-Rochin, V.; Cina, J. A.; Fleming, G. R.; Rice, S. A. *J. Chem. Phys.* **1991**, *95*, 1487. (c) Ziegler, L. D.; Scherer, N. F. *J. Chem. Phys.* **1992**, *97*, 4707.

(21) Nelson, K. A.; Miller, R. J. D.; Lutz, D. R.; Fayer, M. D. *J. Appl. Phys.* **1982**, *53*, 1144.

(22) (a) Robinson, M. M.; Yan, Y.-X.; Gamble Jr., E. B.; Williams, L. R.; Meth, J. S.; Nelson, K. A. *Chem. Phys. Lett.* **1984**, *112*, 491. (b) Farrar, M. R.; Cheng, L.-T.; Yan, Y.-X.; Nelson, K. A. *IEEE J. Quantum Electron.* **1986**, *QE-22*, 1453. (c) DeSilvestri S.; Fujimoto, J. G.; Ippen, E. P.; Gamble Jr., E. B.; Williams, L. R.; Nelson, K. A. *Chem. Phys. Lett.* **1985**, *116*, 146. (d) Williams, L. R.; Gamble Jr., B.; Nelson, K. A.; DeSilvestri S.; Weiner, A.; Ippen, E. P. *Chem. Phys. Lett.* **1987**, *139*, 244.

(23) Cho, M.; Du, M.; Scherer, N. F.; Fleming, G. R.; Mukamel, S. *J. Chem. Phys.* **1993**, *99*, 2410.

(24) Hellwarth, R. W. *Prog. Quantum Electron.* **1977**, *5*, 1.

(25) Levenson, M. D.; Kano, S. S. *Introduction to Nonlinear Spectroscopy*; Academic Press: London, 1988.

(26) (a) Etchepare, J.; Grillon, G.; Chambaret, J. P.; Harmoniaux, G.; Orszag, A. *Opt. Commun.* **1987**, *63*, 329. (b) Deeg, F. W.; Fayer, M. D. *J. Chem. Phys.* **1989**, *91*, 2269.

(27) Kubo, R. In *Fluctuation, Relaxation and Resonance in Magnetic Systems*; terHarr, D., Ed.; Oliver & Boyd: Edinburgh, 1992.

(28) (a) Eesley, G. L.; Levenson, M. D.; Tolles, W. M. *IEEE J. Quantum Electron.* **1978**, *QE-14*, 45. (B) Levenson, M. D.; Eesley, G. L. *Appl. Phys.* **1979**, *19*, 1.

(29) Cho, M.; Rosenthal, S. J.; Scherer, N. F.; Ziegler, L. D.; Fleming, G. R. *J. Chem. Phys.* **1992**, *96*, 5033.

(30) Cho, M.; Fleming, G. R.; Mukamel, S. *J. Chem. Phys.* **1993**, *98*, 5314.

(31) Ziegler, L. D.; Fan, R.; Desroisiers, A. E.; Scherer, N. F. *J. Chem. Phys.* **1994**, *100*, 1823.

(32) Asaki, M. T.; Huang, C. P.; Garvey, D.; Zhou, J.; Kapteyn, H. C.; Murnane, M. *Opt. Lett.* **1993**, *18*, 977.

(33) Duguay, M. A.; Hansen, J. W. *Appl. Phys. Lett.* **1969**, *15*, 192.

(34) Scherer, N. F.; Ziegler, L. D.; Fleming, G. R. *J. Chem. Phys.* **1992**, *96*, 5544.

(35) Wise, F. W.; Rosker, M. J.; Milhauser, G. L.; Tang, C. L. *IEEE J. Quantum Electron.* **1987**, *QE-23*, 1116.

(36) Schrader, B. *Raman/Infrared Atlas of Organic Compounds*; Verlag Chemie: Weinheim, 1990.

(37) Abramowitz, S.; Comeford, J. J. *Spectrochim. Acta* **1965**, *21*, 1479.

(38) (a) Joslin, C. G., Gray, C. G. *Chem. Phys. Lett.* **1989**, *154*, 369. (b) Lund, P. A.; Faourskov Nielsen, O., Praestgaard, E. *Chem. Phys.* **1978**, *28*, 165.

(39) Geiger, L. C.; Ladanyi, B. M. *J. Chem. Phys.* **1987**, *87*, 191.

(40) Hyodo, S.; Tatsuta, N.; Okamoto, T. *J. Chem. Phys.* **1990**, *92*, 882.

(41) Herzberg, G. *Infrared and Raman Spectra*; van Nostrand-Reinhold: New York, 1945.

(42) Fachello, F.; Oss, S. *J. Chem. Phys.* **1993**, *99*, 7337.

(43) Friedman, J. S.; She, C. Y. *J. Chem. Phys.* **1993**, *99*, 4960.

(44) McMorrow, D.; Lotshaw, W. T. *Chem. Phys. Lett.* **1993**, *201*, 369.

(45) Joo, T.; Albrecht, A. C. *J. Chem. Phys.* **1993**, *99*, 3244.

(46) Hayden, C. C.; Trebino, R. *Appl. Phys. B* **1990**, *51*, 350.

(47) Scherer, N. F.; Vöhringer, P.; Ziegler, L. D.; Fleming, G. R., Manuscript in preparation.

(48) Cho, M.; Scherer, N. F.; Fleming; G. R. Mukamel, S. *J. Chem. Phys.* **1992**, *69*, 5618.

(49) Vöhringer, P.; Scherer, N. F. Work in progress.

JP941891Y